Polímeros
ISSN 1678-5169 (Online)

https://doi.org/10.1590/0104-1428.20250112

ORIGINAL ARTICLE

Effect of silica nanoparticles on systems based on polyethylene/offshore-recovered polyamide 11 blends*

Joyce Braga Camargo[1], Gisele Cristina Valle Iulianelli[1], Christine Rabello Nascimento[2] and Ana Lúcia Nazareth da Silva[1,2]*

[1]Instituto de Macromoléculas Professora Eloisa Mano – IMA, Universidade Federal do Rio de Janeiro – UFRJ, Rio de Janeiro, RJ, Brasil

[2]Programa de Engenharia Ambiental – PEA, Universidade Federal do Rio de Janeiro – UFRJ, Rio de Janeiro, RJ, Brasil

**This paper has been partially presented at the 17th Brazilian Polymer Congress, held in Joinville, SC, 29/Oct - 02/Nov/2023.*

**ananazareth@ima.ufrj.br*

Abstract

This study produces and characterizes immiscible blend systems made with high-density polyethylene (HDPE) and post-industrial polyamide 11 (PA11) obtained from offshore. Blends were prepared at an 80/20 (wt.%) HDPE/PA11 ratio. To enhance phase compatibility, high-density polyethylene grafted with maleic anhydride (HDPE-g-MA) was employed as a conventional compatibilizer at 1.5 wt.% content. In addition, the effect of silicon dioxide nanoparticles ($nSiO_2$) incorporated at 2 and 4 wt.% contents was evaluated. The compositions were analyzed in the presence and absence of the compatibilizer. Mechanical, thermal, rheological, and morphological analyses showed that HDPE-g-MA led to a slight improvement in the interfacial interaction between the immiscible polymer phases. Moreover, the addition of $nSiO_2$, in the presence of the traditional compatibilizer, led to the most favorable balance of thermal and mechanical performance, suggesting that $nSiO_2$ nanoparticles may act as effective co-compatibilizers in HDPE/HDPE-g-MA/PA11 systems.

Keywords: *immiscible polymer blends, compatibilization processes, nanocomposites, SiO_2 nanoparticles.*

Data Availability: All data supporting the findings of this study are available from the corresponding author upon request.

How to cite: Camargo, J. B., Iulianelli, G. C. V., Nascimento, C. R., & Silva, A. L. N. (2026). Effect of silica nanoparticles on systems based on polyethylene/offshore-recovered polyamide 11 blends. *Polímeros: Ciência e Tecnologia*, *36*(3), e20260030. https://doi.org/10.1590/0104-1428.20250112.

1. Introduction

Since the emergence of polymeric materials, one of their main advantages over inorganic materials has been their low density. However, due to their relatively weak mechanical and thermal performance compared to metals, for instance, various polymeric systems have been developed to meet increasingly demanding applications[1,2]. To enhance their performance, polymers were progressively reinforced with higher filler loadings, which in turn compromised other properties. From the 1980s onwards, a new class of materials emerged, the polymer nanocomposites, opening new possibilities with the advent of nanotechnology[3].

The performance of polymer blends is significantly influenced by the morphology of the dispersed phase, which can take forms such as spherical particles, fibers, or lamellae[4]. Adding nanofillers to polymeric systems has improved their properties and added new functionalities[5-7]. Lower production costs and better mechanical and barrier properties have led to a lot of research and technological development of these materials[8].

Nanocomposites are defined as multiphase materials in which at least one constituent possesses dimensions within the nanometric scale (0.1-100 nm)[3]. Polymeric nanocomposites are hybrid systems in which a polymer, copolymer, or blend acts as the matrix, and nanofillers are homogeneously dispersed within it. In general, nanocomposites exhibit superior overall performance than neat polymers or regular microcomposites[9-11].

In immiscible polymer blends, the physicochemical and mechanical properties of each polymer remain distinct, and the final material results from the physical combination of two or more incompatible components. However, upon achieving partial miscibility and effective interfacial interactions, synergistic effects may arise, resulting in enhanced or even novel properties that are not observed in the individual polymers[12].

Among the wide variety of nanofillers, silicon dioxide (SiO_2) nanoparticles have been extensively reported as effective additives for polymeric matrices, producing nanocomposites with improved and differentiated properties[13-16].

The present study focuses on the development and evaluation of immiscible polymer systems based on commercial high-density polyethylene (HDPE) and post-industrial polyamide 11 (PA11) from the pressure barrier of flexible pipes. HDPE-g-MA was used as a compatibilizer, and, additionally, the potential compatibilizing or co-compatibilizing role of SiO_2 nanoparticles was investigated. The innovative aspect of this work lies in its dual approach: it explores the reuse of high-performance post-consumer PA11 derived from offshore infrastructure, which is an underexplored source, while simultaneously assessing the synergistic effect of HDPE-g-MA and SiO_2 nanoparticles in tailoring interfacial interactions in HDPE/PA11 blends, aiming at sustainable and high-performance nanocomposite systems.

To contextualize, flexible pipes are key components in offshore oil extraction, as they provide operational adaptability under extreme conditions such as great depths, temperature variations, and intense marine currents[17-20]. These structures consist of multiple polymeric and metallic tubular layers arranged helically (Figure 1). Each layer performs a specific function: while the polymeric layers ensure sealing, the metallic layers provide the mechanical strength required for operation[21-23].

During the service life of these structures, failures may occur, or decommissioning operations may require the removal of flexible pipes from service[24,25]. In both scenarios, although the pressure barriers are typically composed of engineering polymers such as polyamide 11 (PA11), polyamide 12 (PA12), or poly(vinylidene fluoride) (PVDF)[26], these materials are usually discarded without reuse. Therefore, research dedicated to the recycling and valorization of these polymeric barriers aligns with the principles of the Brazilian National Solid Waste Policy (PNRS, 2010), which is defined as an instrument for economic and social development and described as "a set of actions, procedures, and means designed to enable the collection and return of solid waste to the productive sector for reuse in its own production cycle, in other production cycles, or for another environmentally appropriate final destination"[27].

2. Materials and Methods

2.1 Materials

High-density polyethylene (HDPE), grade GM9450F was supplied by Braskem S.A. According to the manufacturer, it is a high-density polyethylene produced with bimodal technology and developed for the high molar mass film extrusion segment and has a melt flow index (MFI) of 9.3 g.10 min^{-1} (based on ASTM D1238 standard) and a density of 0.952 $g.cm^{-3}$ (ASTM D792).

Post-industrial polyamide 11 (PA11) (442 °C - temperature at the maximum degradation rate and Tm = 186 °C – melt temperature) from offshore platforms was donated by Primaplast. The post-industrial pressure barrier was previously cleaned, cut, ground, and subsequently quartered to minimize the expected heterogeneity effect, given that it is a post-consumer material.

Maleic anhydride-grafted HDPE (HDPE-g-MA, 0.4 wt.% maleic anhydride, Mw = 15,000 g/mol) was bought from Sigma Aldrich. Nanosilica (n-SiO_2) type Aerosil R972 (hydrophobic, surface area of 110 ± 20 m^2/g, and particle diameter around 16 nm) was bought from Evonik.

2.2 Blend and composite preparation

Post-industrial PA11 was manually cut and subsequently cryogenically ground in liquid nitrogen (Figure 2). Table 1 lists the experimental formulations utilized in this study. The ratio of HDPE to PA11 was maintained at 80:20. The amount of HDPE-g-MA was set at 1.5 wt.%, while n-SiO_2 was included at either 2 or 4 wt.%. All blends were melt-processed using a co-rotational twin-screw extruder, with a temperature profile ranging from 90 to 200 °C at a speed of 400 rpm.

Test specimens (Type I, ASTM D638) were produced by injection molding (Arburg 270S).

The injection parameters were the temperature range for the barrel zone of 210-250 °C, nozzle temperature of 260 °C, injection pressure of 1600 bar, back pressure of 800 bar, injection speed of 10 $cm^3.s^{-1}$, cooling time of 30 s, and mold temperature of 30 °C.

It is important to highlight that the processing conditions were established based on the thermal behavior of the materials, as determined by thermal analyses, ensuring that the selected temperature range was within the processing window and below degradation temperature.

2.3 Characterizations

Thermogravimetric analysis (TGA) was performed on a Q500 (TA Instruments) equipment under N_2 atmosphere from 30 to 700 °C at 10 °C min^{-1}. The maximum degradation temperature (T_{MAX}) values were determined to assess the thermal stability of the materials.

X-ray diffraction (XRD) was conducted on a Rigaku Ultima IV diffractometer (CuKα, λ = 1.54 Å, 40 kV, 30 mA) over 2θ = 2-80° at 1° min^{-1}. The crystallinity degree (χc) was calculated using Fytik software.

Figure 1. Photo of a typical unbonded flexible riser used in offshore applications, highlighting its main structural layers: interlocked carcasses, pressure armor, tensile armor, pressure barrier, and outer sheath.

Figure 2. Photo of post-industrial PA11 and ground sample.

Table 1. Compositions based on HDPE/PA11—Amounts in wt. %.

Sample Code	HDPE	PA11	HDPE-g-MA	$nSiO_2$
HDPE/PA11	80	20	-	-
HDPE/HDPE-g-AM/PA11	80	20	1.5	-
HDPE/PA11 + 2% $nSiO_2$	80	20	-	2
HDPE/HDPE-g-AM/PA11+ 2% $nSiO_2$	80	20	1.5	2
HDPE/PA11 + 4% $nSiO_2$	80	20	-	4
HDPE/HDPE-g-AM/PA11+ 4% $nSiO_2$	80	20	1.5	4

The surface morphology of the compositions was analyzed using a TESCAN FEG microscope at 10 kV of voltage. Samples were fractured using liquid nitrogen and then coated with gold.

Oscillatory rheology was carried out on an Anton Paar MCR 301 rheometer with 25 mm parallel plates and 1 mm gap at 200 °C. Stress sweep determined the linear viscoelastic region, followed by frequency sweeps (100 Pa, 0.1-600 rad/s) to obtain complex viscosity (η*) and storage modulus (G').

Tensile tests were performed using a universal testing machine (EMIC DL3000) according to ASTM D638 (Type I) at a crosshead speed of 50 mm min-1. This test was replicated 5 times.

Data were analyzed using STATISTICA 6. ANOVA verified significant differences, with residual normality and variance homogeneity tested. Fisher's LSD test was applied at $\alpha = 0.05$.

3. Results and Discussion

3.1 Thermal analysis

The thermal stability of the HDPE/PA11 systems, with and without n-SiO_2 nanoparticles, was evaluated based on their T_{MAX} values, as presented in Table 2.

Table 2. TGA results of the HDPE/PA11 compositions.

Sample Code	T_{MAX} (°C) ± 2 °C
HDPE/PA11	467
HDPE/HDPE-g-AM/PA11	461
HDPE/PA11 + 2% $nSiO_2$	479
HDPE/HDPE-g-AM/PA11+ 2% $nSiO_2$	482
HDPE/PA11 + 4% $nSiO_2$	466
HDPE/HDPE-g-AM/PA11+ 4% $nSiO_2$	479

Although HDPE-g-MA is recognized to be an efficient compatibilizer for HDPE and PA11 blends[12-14], a reduction in T_{MAX} for the HDPE/PA11 blend was observed (Table 2) and showed in the TGA/DTG thermograms (Figure 3). This decrease in thermal behavior can be attributed to the fact that the PA11 used in this study is a post-industrial material; therefore, it was exposed to oil during service, which could have impaired the compatibilization efficiency of HDPE-g-MA.

The addition of 2% wt. of $nSiO_2$ to the HDPE/PA11 blend led to a rise in T_{MAX} value (approximately 12 °C), indicating enhanced thermal stability. This behavior can be attributed to the barrier effect promoted by well-dispersed nanoparticles, which restrict the diffusion of volatile degradation products

and delay thermal decomposition[1,7,26]. In the compatibilized system (presence of the compatibilizer agent), the addition of 2 wt.% $nSiO_2$ resulted in a slightly higher increase in T_{MAX} (15 °C), suggesting a synergistic effect between HDPE-g-MA and the nanoparticles, improving interfacial adhesion and dispersion[1,4,28].

At higher nanoparticle loading (4 wt.%), no significant increase in T_{MAX} was observed for the non-compatibilized blend, likely due to nanoparticle agglomeration, which reduces the effective surface area and limits the barrier effect[6,25]. In contrast, in the presence of the compatibilizer, the addition of 4 wt.% $nSiO_2$ still promoted an increase in T_{MAX}, although comparable to that observed at the composition without the compatibilizing agent. This result suggests that HDPE-g-MA contributes to a more effective dispersion of nanoparticles, even at higher loadings, maintaining their stabilizing effect[1,28].

It is important to note that PA11 used in this study is a post-industrial material, which may introduce some variability in the results due to differences in prior processing and service history[13,16]. However, to minimize heterogeneity, the PA11 was previously ground to improve its dispersion within the HDPE matrix. Therefore, the observed thermal behavior is primarily associated with morphological factors, such as nanoparticle dispersion and interfacial interactions, rather than solely the previous exposure conditions of the PA11.

It is also important to highlight that the mass loss observed in the temperature range between 30-250 °C refers to the loss of plasticizer, normally present in commercial grades of PA11 used in the manufacture of pressure barriers.

3.2 Morphology – SEM analysis

Figure 4 shows the SEM micrographs of neat HDPE, HDPE/PA11 blends with and without compatibilizer, and HDPE/PA11/$nSiO_2$ composites with and without compatibilizer.

According to Figure 4a, the HDPE/PA11 binary blend has typical island-sea-type morphology, where irregular droplets (island phase) are dispersed in the HDPE matrix (sea phase). When the compatibilizer (HDPE-g-MA) was added to the HDPE/PA11 binary blend (Figure 4b), the droplets of PA11 seem to have become more uniform, although there is no evidence of having an effective interaction between the HDPE and PA11 phases. Further, adding 2% and 4% wt. $nSiO_2$ to the HDPE/HDPE-g-MA/PA11 blends (Figures 4d and 4f) changed the PA11 dispersed phase morphology compared to the HDPE/PA11 blends containing the same amount of $nSiO_2$ but without HDPE-g-MA (Figures 4c and 4e). The dispersed phase of PA11 becomes more uniform and well dispersed in the HDPE matrix, indicating an improvement in interaction between the HDPE and PA11 phases. Similar behavior was reported in the literature for an HDPE/PLA blend with HDPE-g-MA compatibilizer and $CaCO_3$ nanoparticles ($nCaCO_3$)[29]. In that study, the authors reported that a reduction in the interfacial tension caused a synergistic effect of HDPE-g-MA and $nCaCO_3$. The morphologies observed in Figure 4 also suggest the synergistic effect of the SiO_2 nanoparticles and HDPE-g-MA on the interaction between the immiscible phases, HDPE and PA11. These evaluations corroborate the previously discussed results (Table 2), indicating that, in the presence of the HDPE-g-MA, $nSiO_2$ can act as a co-compatibilizer for the HDPE/PA11 blend.

3.3 X-ray diffraction (XRD) analysis

Figure 5 presents the X-ray diffraction patterns of the raw materials: HDPE (a), PA11 (b), and $nSiO_2$ (c). The diffractograms of the processed materials, including neat HDPE, PA11, $nSiO_2$, and the HDPE/PA11 blends and composites, are shown in Figure 5d.

The crystalline peaks of PA11 are observed at diffraction angles (2θ) of 20.2°, corresponding to the (100) crystal plane, and at 23.5°, corresponding to the (010) and (110) planes, which are characteristic of the triclinic α-form arrangement[30]. HDPE has a strong reflection peak at 21.6° and a weaker one at 24.0°. These peaks correspond to the orthorhombic unit cell structure of the (110) and (200) reflection planes, respectively. These 2θ values are consistent with those reported in the literature[28].

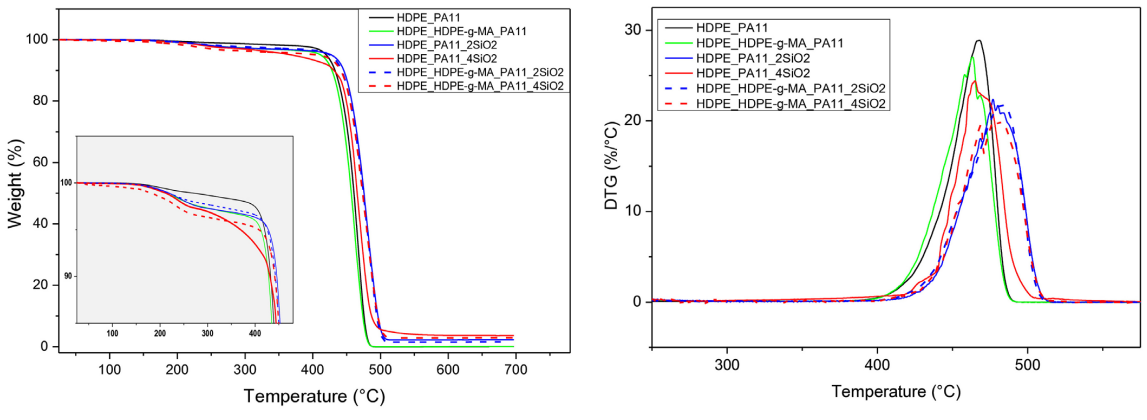

Figure 3. (a) TGA curves and (b) DTG curves of HDPE/PA11 compositions.

There are two more weak peaks at about 30.0° and 36.2°, which are caused by the (210) and (020) planes, respectively. There are also a few other small reflections in the 38°-60° range[28]. The commercial nanosilica, Aerosil® R972, exhibits a broad amorphous profile, lacking distinct reflections from crystalline planes, which indicates its amorphous morphology. Literature suggests that more crystalline forms would show peaks at 13° (020), 17° (110), and 30.7° (002)[2].

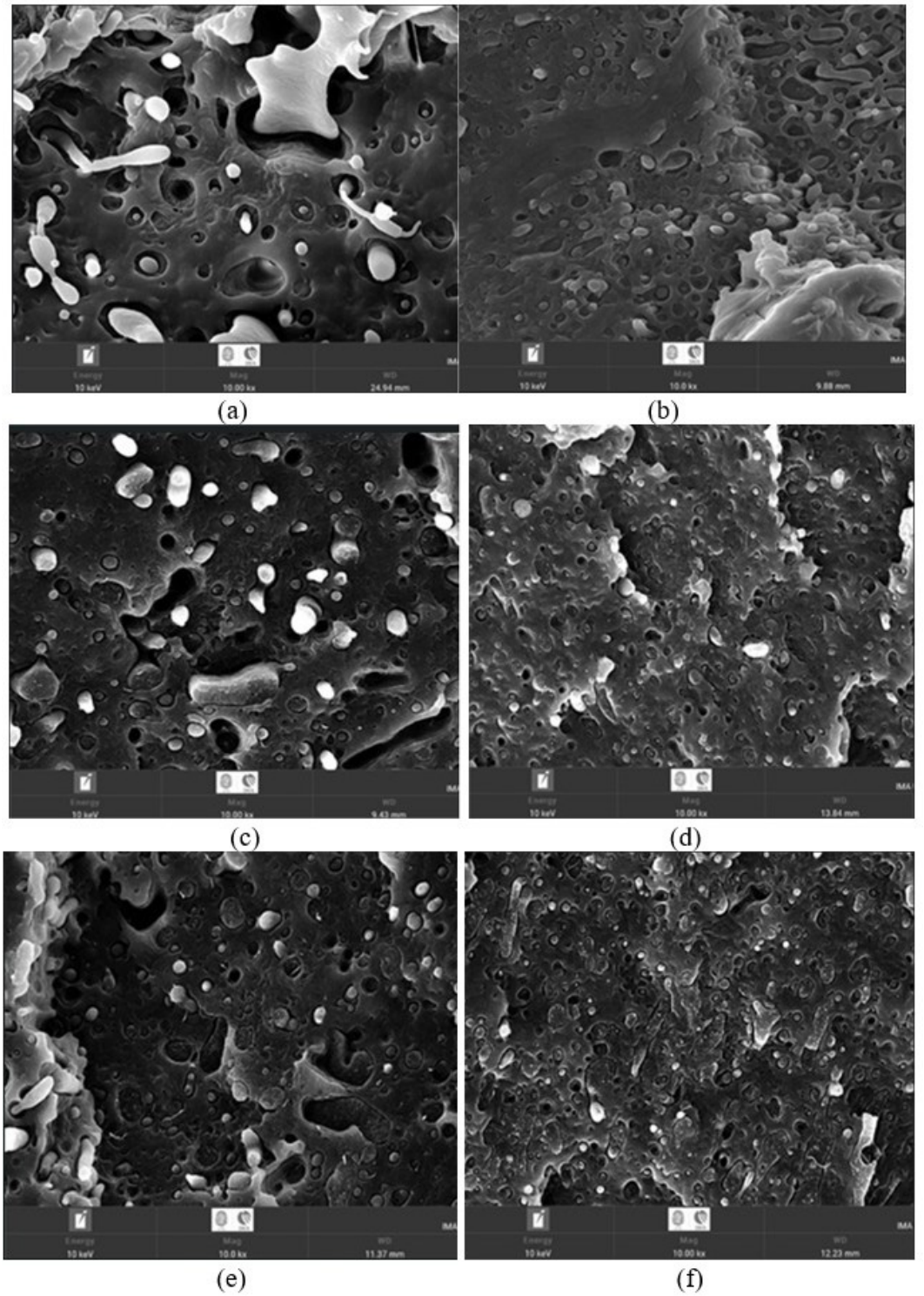

Figure 4. SEM micrographs of (a) HDPE/PA11, (b) HDPE/HDPE-g-MA/PA11, (c) HDPE/PA11 + 2% $nSiO_2$, (d) HDPE/HDPE-g-AM/PA11+ 2% $nSiO_2$, (e) HDPE/PA11 + 4% $nSiO_2$, and (f) HDPE/HDPE-g-AM/PA11+ 4% $nSiO_2$.

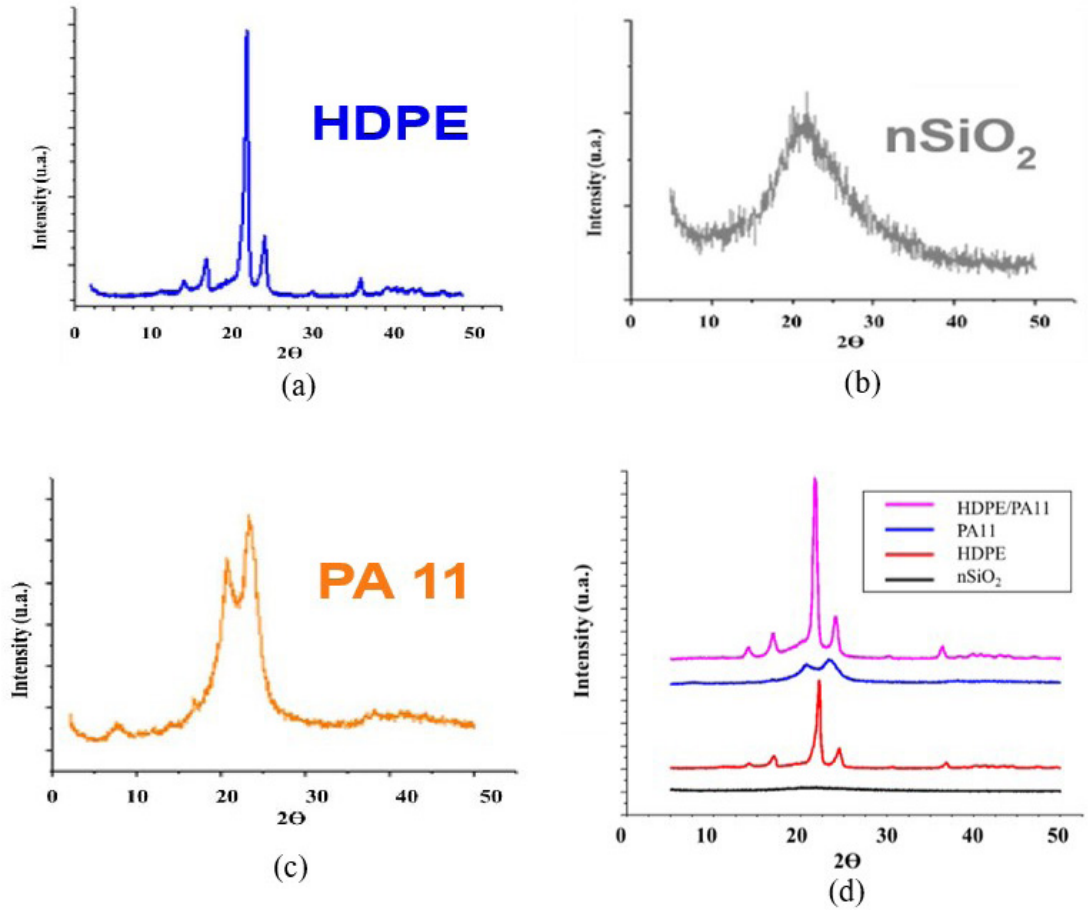

Figure 5. X-ray diffraction patterns (a) HDPE, (b) $nSiO_2$, (c) PA11 and (d) neat HDPE, PA11, $nSiO_2$, and HDPE/PA11 blend.

The diffractograms show that the HDPE/PA11 blend exhibits peak positions similar to those of the individual neat polymers. The HDPE/PA11 blend shows the typical HDPE reflection peaks, with a strong signal at 21.6° and a weaker one at 24.0°, assigned to the (110) and (200) planes of the orthorhombic unit cell[28]. The weaker reflections at $2\theta \approx 30.0°$ and 36.2° correspond to the (210) and (020) planes, respectively, and minor reflections are also visible in the 38-60° range[30]. The characteristic HDPE peaks in HDPE/PA11 exhibit an amorphous halo, attributed to the overlapping PA11 phase peaks.

Figure 6 compares the diffractograms of HDPE/PA11 blends, with and without the HDPE-g-MA compatibilizer, and composites based on HDPE/PA11/$nSiO_2$ with and without the commercial compatibilizer.

Figure 6 illustrates that the two primary crystalline peaks located at 21.6° (110) and 24.0° (200) of HDPE exhibited no significant changes in intensity following the addition of the compatibilizing agent. In contrast, the intensity of these peaks decreased in systems containing $nSiO_2$ nanofiller, regardless of the presence of the compatibilizing agent. This reduction was particularly pronounced in the systems with both the compatibilizing agent and nanoparticles, highlighting the synergistic effect of HDPE-g-MA and $nSiO_2$ in enhancing the interaction between the HDPE and PA11 phases. Table 3 shows the crystallinity degree of the samples calculated from XRD data.

Table 3 shows that the addition of PA11 to HDPE causes a decrease in its crystallinity degree, indicating that the presence of the dispersed PA11 phase hinders the growth of HDPE crystals. With the addition of the compatibilizing agent, there was a more pronounced decrease in crystallinity degree, indicating a greater impediment to crystal growth, probably due to interaction between the HDPE and PA11 phases. The lowest crystallinity values are observed in the HDPE/HDPE-g-MA/PA11 composites containing 2 wt.% and 4 wt.% $nSiO_2$, suggesting a strengthened interphase interaction. This behavior is consistent with literature findings in which hydrophobic nanosilica combined with compatibilizers reduces crystallinity by localizing at the polymer's interface, restricting chain mobility, and thus reducing the ability of HDPE chains to organize into crystals[26,31,32].

3.4 Oscillatory rheology

Oscillatory rheology was utilized to assess the viscoelastic properties of the polymeric systems. Low-frequency measurements yield important insights into the phase structure and the effectiveness of dispersion within the blends[26].

Figures 7 and 8 illustrate, respectively, the complex viscosity (η*) and storage modulus (G′) as a function of frequency for HDPE/PA11, both with and without a compatibilizer, as well as for HDPE/PA11/nSiO$_2$ compositions, which also vary in the presence of the HDPE-g-MA compatibilizer and different amounts of SiO$_2$ nanoparticles.

The addition of HDPE-g-MA increased the elastic response of the blends, indicating higher flow restriction and improved interfacial adhesion between the polymer phases[27].

Table 3. Crystallinity degree (χ_c) of neat HDPE and HDPE/PA11 compositions.

Sample Code	χ_c (%)
Neat HDPE	66
HDPE/PA11	60
HDPE/HDPE-g-AM/PA11	56
HDPE/PA11 + 2% nSiO$_2$	53
HDPE/HDPE-g-AM/PA11+ 2% nSiO$_2$	45
HDPE/PA11 + 4% nSiO$_2$	54
HDPE/HDPE-g-AM/PA11+ 4% nSiO$_2$	48

The incorporation of SiO$_2$ nanoparticles also affected the viscoelastic behavior, as shown by the increased values of both complex viscosity (Figure 7) and storage modulus (Figure 8) at low frequencies. This behavior suggests that the nanofiller promotes higher phase interaction, even in the absence of the compatibilizer, due to possible physical interactions between the polar groups of PA11 and the surface hydroxyl groups of the silica nanoparticles[28,30,31].

Oscillatory rheology is a key technique for assessing the viscoelastic nature of polymer blends, enabling the correlation of rheological responses with the morphological structure and phase dispersion. The results indicate that the compatibilized systems exhibit more elastic characteristics, especially at low frequencies, confirming the enhanced interfacial adhesion provided by HDPE-g-MA and nSiO$_2$ nanoparticles in the HDPE/PA11 matrix[28].

3.5 Tensile properties

Tensile testing results are presented in Table 4. The mechanical properties of the HDPE/PA11 blends were evaluated by tensile testing, showing that the addition of nSiO$_2$ generally increased tensile strength, stress at break, and elastic modulus.

Table 4. Mechanical properties of neat HDPE, HDPE/PA11 and HDPE/HDPE-g-MA/PA11 compositions, with different contents of nSiO$_2$.

Sample Code	Stress at break (MPa)*	Elastic Modulus (MPa)*	Strain at Break (%)*
HDPE/PA11	9.0	667	58
HDPE/HDPE-g-AM/PA11	9.3	649	72
HDPE/PA11 + 2% nSiO$_2$	12.0	713	41
HDPE/HDPE-g-AM/PA11+ 2% nSiO$_2$	11.7	746	75
HDPE/PA11 + 4% nSiO$_2$	11.5	695	42
HDPE/HDPE-g-AM/PA11+ 4% nSiO$_2$	11.2	751	79

*The values had been verified by performing ANOVA, and a confidence interval of 0.95 was applied.

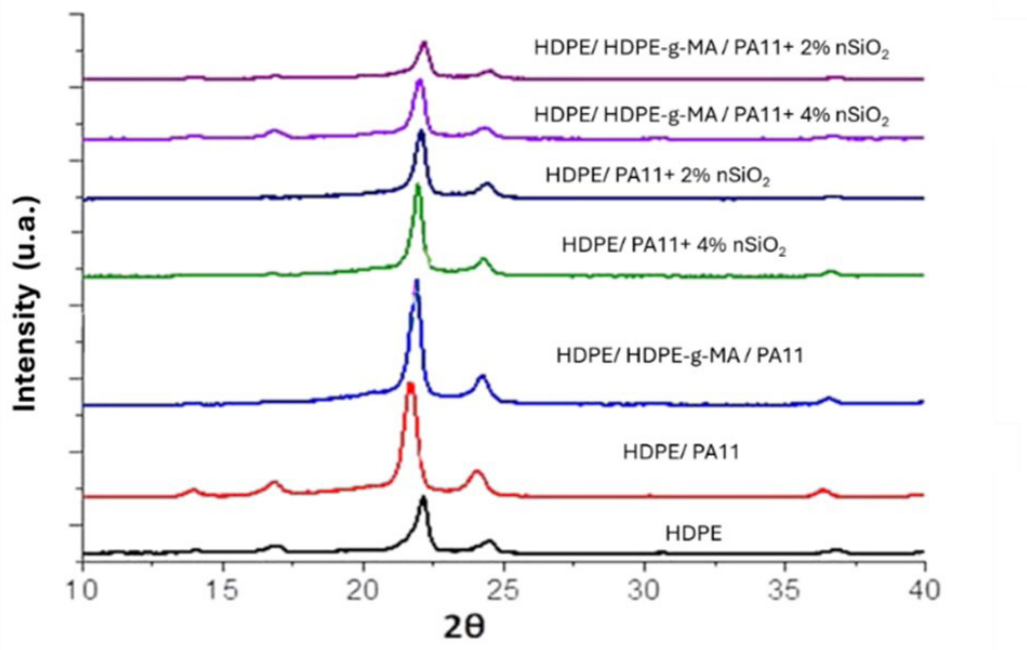

Figure 6. Diffractograms of neat HDPE and HDPE/PA11 compositions.

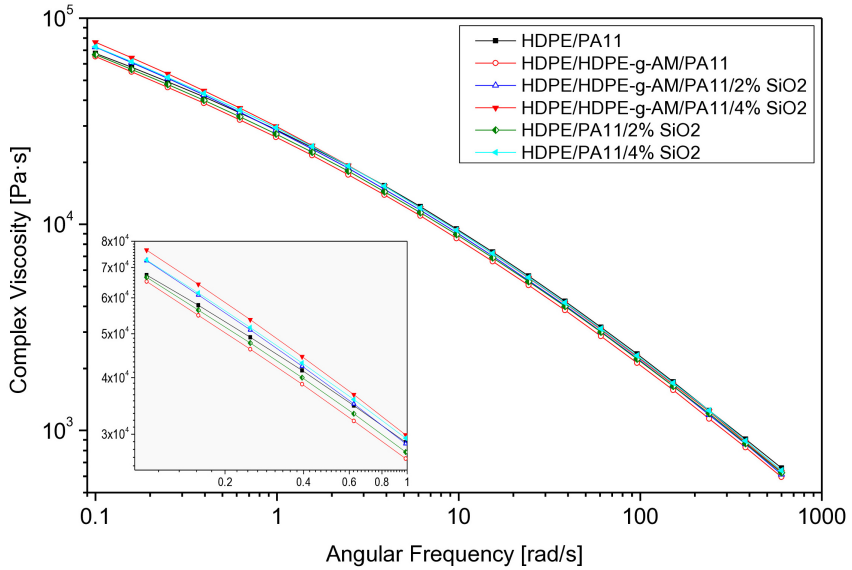

Figure 7. Rheology curves of complex viscosity (η*) versus frequency for HDPE/PA11 and HDPE/HDPE-g-MA/PA11 blends containing 2 wt% and 4 wt% $nSiO_2$.

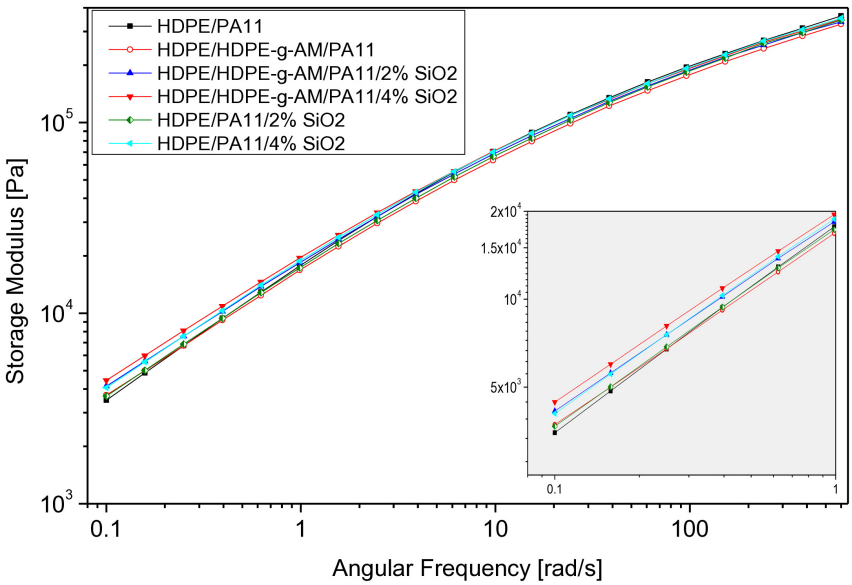

Figure 8. Rheology curves of storage modulus (G′) *versus* frequency for HDPE/PA11 and HDPE/HDPE-g-MA/PA11 blends containing 2 wt% and 4 wt% $nSiO_2$.

Based on the Fisher LSD statistical test, the mean values of stress at break of samples with $nSiO_2$ were statistically similar to each other but significantly higher than the HDPE/PA11 matrix, indicating that the nanofiller, with or without HDPE-g-MA, enhances mechanical performance[4,7,26]. Regarding the elastic modulus and strain at break properties, statistical analysis revealed that the HDPE/PA11 compositions with $nSiO_2$ nanofiller tend to present the lower values compared to the composites with the presence of the compatibilizing agent, signaling a co-compatibilizing effect of the nanoparticles with the commercial compatibilizer in the tensile properties. It is important to highlight that HDPE/HDPE-g-MA/PA11 systems with the addition of $nSiO_2$ exhibit greater toughness compared to other compositions.

Overall, the mechanical, rheological, and thermal performance of the HDPE/PA11/n-SiO_2 blends suggests that the addition of SiO_2 nanofiller with HDPE-g-MA provides an optimal combination of tensile strength, flow properties, and thermal stability, making these materials promising for injection-molded applications in construction and other industrial uses.

4. Conclusions

This study developed and characterized immiscible blend systems based on high-density polyethylene (HDPE) and post-industrial polyamide 11 (PA11) sourced from offshore pressure barriers. The addition of HDPE-grafted with maleic anhydride (HDPE-g-MA) as a compatibilizer improved interfacial adhesion between the polymer phases, although only modest enhancements were observed. Incorporation of silicon dioxide nanoparticles ($nSiO_2$) at 2 and 4 wt.% further influenced blend properties, with 2 wt.% $nSiO_2$ yielding a significant increase in thermal stability due to improved nanoparticle dispersion and barrier effects. The synergistic combination of HDPE-g-MA and $nSiO_2$ was particularly effective, resulting in the best balance of mechanical strength, toughness, and thermal performance.

Morphological analysis revealed that compatibilized blends containing $nSiO_2$ exhibited a more uniform and well-dispersed PA11 phase within the HDPE matrix, confirming enhanced phase interaction. X-ray diffraction demonstrated a reduction in crystallinity degree associated with the presence of PA11 and further decreased by the addition of compatibilizer and nanoparticles, indicating strengthened interphase interactions and restricted chain mobility.

Rheological results showed that compatibilized blends and nanocomposites displayed increased elastic modulus and complex viscosity values, especially at low frequencies, verifying improved interfacial adhesion and phase dispersion. Tensile tests confirmed that blends incorporating $nSiO_2$, with or without HDPE-g-MA, achieved higher mechanical performance, with the best toughness and modulus observed in systems containing both additives.

Overall, the findings demonstrate that $nSiO_2$ nanoparticles act as effective co-compatibilizers in HDPE/HDPE-g-MA/PA11 blends, enabling the production of sustainable, high-performance nanocomposites suitable for injection-molded applications. The reuse of post-industrial PA11 aligns with circular economy principles, offering promising routes for the valorization of engineering polymers from offshore infrastructure.

5. Author's Contribution

- **Conceptualization** – Joyce Braga Camargo; Ana Lúcia Nazareth da Silva; Gisele Cristina Valle Iulianelli.
- **Data curation** – Joyce Braga Camargo; Christine Rabello Nascimento.
- **Formal analysis** – Joyce Braga Camargo.
- **Funding acquisition** – Joyce Braga Camargo; Ana Lúcia Nazareth da Silva; Gisele Cristina Valle Iulianelli.
- **Investigation** – Joyce Braga Camargo.
- **Methodology** – Joyce Braga Camargo; Ana Lúcia Nazareth da Silva; Gisele Cristina Valle Iulianelli.
- **Project administration** – Joyce Braga Camargo; Ana Lúcia Nazareth da Silva; Gisele Cristina Valle Iulianelli.
- **Resources** – Joyce Braga Camargo; Ana Lúcia Nazareth da Silva; Gisele Cristina Valle Iulianelli.
- **Software** – NA.
- **Supervision** – Ana Lúcia Nazareth da Silva; Gisele Cristina Valle Iulianelli.
- **Validation** – Joyce Braga Camargo; Christine Rabello Nascimento; Ana Lúcia Nazareth da Silva; Gisele Cristina Valle Iulianelli.
- **Visualization** – Joyce Braga Camargo.
- **Writing – original draft** – Joyce Braga Camargo.
- **Writing – review & editing** – Joyce Braga Camargo; Ana Lúcia Nazareth da Silva.

6. Acknowledgements

The authors acknowledge the Conselho Nacional de Desenvolvimento Científico e Tecnológico (CNPQ) (307889/2022) and Coordenação de Aperfeiçoamento de Pessoal de Nível Superior - CAPES.

7. References

1. Taguet, A., Cassagnau, P., & Lopez-Cuesta, J.-M. (2014). Structuration, selective dispersion and compatibilizing effect of (nano)fillers in polymer blends. *Progress in Polymer Science*, *39*(8), 1526-1563. https://doi.org/10.1016/j.progpolymsci.2014.04.002.
2. Rodriguez, A. O. F., Silva, P. S. R. C., Iulianelli, G. C. V., & Tavares, M. I. B. (2021). Effect of silicon dioxide in the PHB matrix characteristics. *International Journal of Developmental Research*, *11*(2), 44179-44183. Retrieved in 2025, December 20, from https://www.journalijdr.com/sites/default/files/issue-pdf/21038.pdf
3. Lindsay, S. M. (2009). Introduction to nanoscience. Oxford: Oxford University Press.. https://doi.org/10.1093/oso/9780199544202.001.0001.
4. Liu, S., Li, C., Wu, H., & Guo, S. (2020). Novel structure to improve mechanical properties of polymer blends: multilayered ribbons. *Industrial & Engineering Chemistry Research*, *59*(45), 20221-20231. https://doi.org/10.1021/acs.iecr.0c04448.
5. Mazinani, S., Darvishmanesh, S., Ramazani, R., & Van der Bruggen, B. (2017). Miscibility of polyimide blends: physicochemical characterization of two high-performance polyimide polymers. *Reactive & Functional Polymers*, *111*, 88-101. https://doi.org/10.1016/j.reactfunctpolym.2016.12.010.
6. Zare, Y. (2016). Modeling the yield strength of polymer nanocomposites based upon nanoparticle agglomeration and polymer–filler interphase. *Journal of Colloid and Interface Science*, *467*, 165-169. https://doi.org/10.1016/j.jcis.2016.01.022. PMid:26802275.
7. Peponi, L., Puglia, D., Torre, L., Valentini, L., & Kenny, J. M. (2014). Processing of nanostructured polymers and advanced polymeric-based nanocomposites. *Materials Science and Engineering R Reports*, *85*, 1-46. https://doi.org/10.1016/j.mser.2014.08.002.
8. Rodrigues, A. C., Bastos, I. N., Kappel, M. A. A., Nascimento, C. R., Ferreira, L. S., & Silva, A. L. N. (2021). Micromechanical property study of nylon 11 and organoclay systems for offshore flexible pipe. *Fibers and Polymers*, *22*(11), 3172-3182. https://doi.org/10.1007/s12221-021-0391-5.
9. Yu, Z.-Z., Hu, G.-H., Varlet, J., Dasari, A., & Mai, Y.-W. (2005). Water-assisted melt compounding of nylon 6/pristine montmorillonite nanocomposites. *Journal of Polymer Science. Part B, Polymer Physics*, *43*(9), 1100-1112. https://doi.org/10.1002/polb.20397.
10. Custódio, A. B., & Vaz, M. A. (2002). A nonlinear formulation for the axisymmetric response of umbilical cables and flexible pipes. *Applied Ocean Research*, *24*(1), 21-29. https://doi.org/10.1016/S0141-1187(02)00007-X.

11. Fergestad, D., & Løtveit, S. A. (Eds.). (2017). *Handbook on design and operation of flexible pipes*. Trondheim: SINTEF.
12. Guimarães, M. G. B. (2013). *Dependência da fluência e recuperação do fluoreto de polivinilideno (PVDF) com a temperatura e taxa de recuperação* (Monografia). Universidade Federal do Rio de Janeiro, Rio de Janeiro. Retrieved in 2025, December 20, from https://monografias.poli.ufrj.br/monografias/monopoli10006017.pdf
13. Rodrigues, A. C., Kappel, M. A. A., Nascimento, C. R., Spinelli, L. S., Bastos, I. N., & Silva, A. L. N. (2016). Modeling instrumented indentation testing to evaluate the behavior of PA11 and $CaCO_3$ composites for offshore applications. *Polymer Testing*, *56*, 140-147. https://doi.org/10.1016/j.polymertesting.2016.10.003.
14. Morais, J. M. (2013). *Deepwater petroleum: a technological history of Petrobras in offshore exploration and production.* Brasília: Instituto de Pesquisa Econômica Aplicada. Retrieved in 2025, December 20, from http://repositorio.ipea.gov.br/handle/11058/1147
15. Zhang, Y., Chen, B., Qiu, L., Hill, T., & Case, M. (2003). *State of the art analytical tools improve optimization of unbonded flexible pipes for deepwater environments.* In *Offshore Technology Conference*, Houston, TX, USA. Richardson, TX: OnePetro. https://doi.org/10.4043/15169-MS.
16. Sudaia, D. P., Bastos, M. B., Fernandes, E. B., Nascimento, C. R., Pacheco, E. B. A. V., & Silva, A. L. N. (2018). Sustainable recycling of mooring ropes from decommissioned offshore platforms. *Marine Pollution Bulletin*, *135*, 357-360. https://doi.org/10.1016/j.marpolbul.2018.06.066. PMid:30301047.
17. Rouse, S., Hayes, P., Davies, I. M., & Wilding, T. A. (2018). Offshore pipeline decommissioning: scale and context. *Marine Pollution Bulletin*, *129*(1), 241-244. https://doi.org/10.1016/j.marpolbul.2018.02.041. PMid:29680543.
18. Park, M. S., Lee, S., Kim, A. R., Choi, I., Shin, J., & Kim, Y.-W. (2019). Toughened and hydrophobically modified polyamide 11 copolymers with dimer acids derived from waste vegetable oil. *Journal of Applied Polymer Science*, *136*(10), 47174. https://doi.org/10.1002/app.47174.
19. Filippone, G., Carroccio, S. C., Curcuruto, G., Passaglia, E., Gambarotti, C., & Dintcheva, N. T. (2015). Time-resolved rheology as a tool to monitor the progress of polymer degradation in the melt state: part II—thermal and thermo-oxidative degradation of polyamide 11/organo-clay nanocomposites. *Polymer*, *73*, 102-110. https://doi.org/10.1016/j.polymer.2015.07.042.
20. Cai, J., Jiang, X., & Lodewijks, G. (2017). Residual ultimate strength of offshore metallic pipelines with structural damage: a literature review. *Ships and Offshore Structures*, *12*(8), 1037-1055. https://doi.org/10.1080/17445302.2017.1308214.
21. Zheng, X., Zheng, S., Zhang, X., Yang, W., Liu, Z., & Yang, M. (2016). Phase morphology control and selective localization of MWCNT for suppressing dielectric loss and enhancing the dielectric constant of HDPE/PA11/MWCNT composites. *RSC Advances*, *6*(77), 73056-73062. https://doi.org/10.1039/C6RA13127A.
22. Zhou, C., Wang, K., & Fu, Q. (2009). Toughening of polyamide 11 via addition of crystallizable polyethylene derivatives. *Polymer International*, *58*(5), 538-544. https://doi.org/10.1002/pi.2564.
23. Liu, Q., Qu, Z., Chen, F., Liu, X., & Wang, G. (2024). Review of the development of an unbonded flexible riser: new material, types of layers, and cross-sectional mechanical properties. *Materials*, *17*(11), 2560. https://doi.org/10.3390/ma17112560. PMid:38893824.
24. Lyu, Y., Pang, J., Gao, Z., Zhang, Q., & Shi, X. (2019). Characterization of the compatibility of PVC/PLA blends by aid of rheological responses. *Polymer*, *176*, 20-29. https://doi.org/10.1016/j.polymer.2019.05.016.
25. Jin, J., Rafiq, R., Gill, Y. Q., & Song, M. (2013). Preparation and characterization of high-performance graphene/nylon nanocomposites. *European Polymer Journal*, *49*(9), 2617-2626. https://doi.org/10.1016/j.eurpolymj.2013.06.004.
26. Laoutid, F., François, D., Paint, Y., Bonnaud, L., & Dubois, P. (2013). Using nanosilica to fine-tune morphology and properties of polyamide 6/poly(propylene) blends. *Macromolecular Materials and Engineering*, *298*(3), 328-338. https://doi.org/10.1002/mame.201200047.
27. Brasil. *Lei nº 12.305, de 2 de agosto de 2010*. (2010, 2 de agosto). Institui a Política Nacional de Resíduos Sólidos. Diário Oficial da República Federativa do Brasil, Brasília. Retrieved in 2025, December 20, from http://www.planalto.gov.br/ccivil_03/_ato2007-2010/2010/lei/l12305.htm
28. Palacios, J. K., Sangroniz, A., Eguiazabal, J. I., Etxeberria, A., & Müller, A. J. (2016). Tailoring the properties of PP/PA6 nanostructured blends by the addition of nanosilica and compatibilizer agents. *European Polymer Journal*, *85*, 532-552. https://doi.org/10.1016/j.eurpolymj.2016.11.010.
29. Oliveira, A. G., Silva, A. L. N., Sousa, A. M. F., Leite, M. C. A. M., Jandorno, J. C., & Escócio, V. A. (2016). Composites based on green high-density polyethylene, polylactide and nanosized calcium carbonate: effect of the processing parameter and blend composition. *Materials Chemistry and Physics*, *181*, 344-351. https://doi.org/10.1016/j.matchemphys.2016.06.068.
30. Chouit, F., Guellati, O., Boukhezar, S., Harat, A., Guerioune, M., & Badi, N. (2014). Synthesis and characterization of HDPE/N-MWNT nanocomposite films. *Nanoscale Research Letters*, *9*(1), 288. https://doi.org/10.1186/1556-276X-9-288. PMid:25024676.
31. Sangroniz, L., Moncerrate, M. A., De Amicis, V. A., Palacios, J. K., Fernández, M., Santamaria, A., Sánchez, J. J., Laoutid, F., Dubois, P., & Müller, A. J. (2015). The outstanding ability of nanosilica to stabilize dispersions of nylon 6 droplets in a polypropylene matrix. *Journal of Polymer Science. Part B, Polymer Physics*, *53*(22), 1567-1579. https://doi.org/10.1002/polb.23786.
32. Jeziorska, R., Szadkowska, A., & Studzinski, M. (2022). Morphology and properties of poly(2,6-dimethyl-1,4-phenylene oxide)/polyamide 11 hybrid nanocomposites: effect of silica surface modification. *Materials*, *15*(10), 3421. https://doi.org/10.3390/ma15103421. PMid:35629449.

Received: Dec. 20, 2025
Revised: Apr. 08, 2026
Accepted: May 19, 2026

Associate Editor: *Artur J. M. Valente*